JOURNAL OF MATERIALS SCIENCE 12 (1977) 1401–1410

A fracture approach to thick film adhesion measurements

W. D. BASCOM, J. L. BITNER
Surface Chemistry Branch, Naval Research Laboratory, Washington D. C., USA

The constant-compliance double cantilever beam test for adhesive fracture energy has been adapted to the measurement of the adhesion of thick film metallizations on alumina. The test involves a single beam soldered to metallization strips and measures the opening-mode fracture energy, $\mathcal{G}_{Ic}$. Solder-wire peel tests were also made on the same metallizations. Both the fracture and peel tests indicated failure in the thick films but near the film/alumina boundary and both sets of data exhibited a bimodal distribution. The magnitude of the fracture energies indicated failure usually occurred in the glass phase of the film but that film adherence was greatly enhanced by interlocking between the metal and glass phases. This interlocking, and thus the film adhesion, was strongly dependent on the firing temperature.

1. Introduction

The technology of thick film metallizations in hybrid microcircuitry defies all but a phenomenological description. Ink formulation, screen printing and firing are largely empirical processes that have evolved from commerical practice. None the less, there has been some progress in developing scientific insights into thick film technology. For example, the work of Vest *et al.* [1] on the printing and firing process and conduction mechanisms, and Hitch [2, 3] on the relationship between film morphology and the bond strength of connector leads.

The work reported here was on the thick film, conductive metallizations. These films are formed on ceramic substrates by screen printing inks containing metal powders, glass frits of Si, B, Pb, Bi and other metals, and an organic vehicle. The printings are fired and in the process the vehicle is driven off, the metallic constituents are at least partially sintered together and the glass forms a bonding layer between the metal conductive and the substrate.

The adhesion of thick films to ceramic substrates is a matter of particular concern since it affects the reliability of the microelectronic device. The term "adhesion" is used broadly here to refer to the failure strength of separating film from substrate. Failure need not occur along the boundary between the two phases and in fact such interfacial failure is unlikely although separation may occur deceptively close to the interface [4].

The methods that have been used to test the adhesion of thick films [5] are generally the same as have been used for the thin, evaporated metal films [6] such as the "scotch" tape peel test, scratch tests and cleavage tests. A test that has gained wide use in the thick film industry is the duPont solder bond peel test [7].

All of the test methods currently in use give results that are useful for purposes of comparison and are valuable for ranking the adhesion of different inks or for quality control purposes. However, the test data have no inherent significance with respect to material strength. In this paper a technique is described for determining the "adhesive" fracture energy of thick film metallization. The results can, in principle be related to the fracture energies and other properties of the materials of which the film and substrate are composed. Moreover, the fracture data combined with detailed post-failure examination give insight into failure mechanisms. A companion study of thick film adhesive fracture also conducted at this laboratory, but using a different specimen configuration, has been reported recently [8].

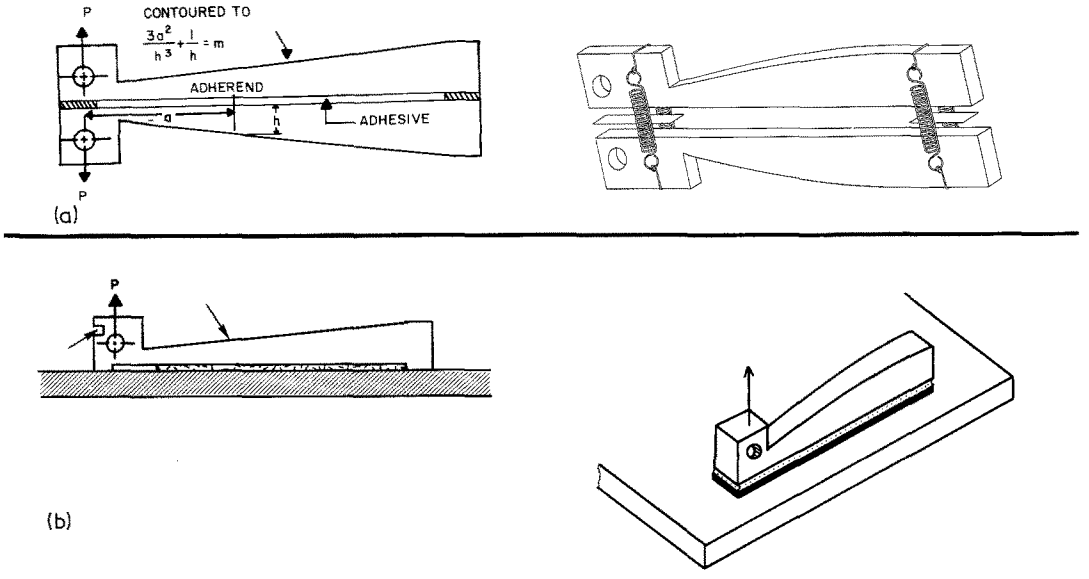

Figure 1(a) Plan and schematic diagrams of constant compliance double cantilever beam adhesive fracture specimen [8, 9]. (b) Plan and schematic diagrams of constant compliance single beam specimen for thick film adhesive fracture. Thin arrows indicate tension and compression points for pre-cracking.

2. Experimental details

2.1. Constant compliance fracture test

One of the principal test methods for measuring adhesive fracture on commercial adhesives employs a tapered double cantilever beam test specimen illustrated in Fig. 1a [9, 10]. The two beams, usually made of aluminium, are bonded by the organic adhesive. The short strips of tape (Teflon) at the ends maintain the desired bond thickness and the springs hold the specimen together during heat cure of the adhesive. The force required to open the beams is measured and used to calculate the opening mode (cleavage or mode-I) fracture energy. The general relationship for mode-I fracture is

$$\mathcal{G}_{Ic} = \frac{P_c^2}{2b}\left(\frac{dC}{da}\right)_P, \qquad (1)$$

where $\mathcal{G}_{Ic}$ is the opening mode strain energy release rate and is equal to the fracture energy, C is the compliance, P_c is the failure load, and a is the crack length. For a rectangular beam, Equation 1 becomes, from simple beam theory,

$$\mathcal{G}_{Ic} = \frac{4P_c^2}{b^2E_b}\left[\frac{3a^2}{h^3}+\frac{1}{h}\right], \qquad (2)$$

where E_b is the bending modulus of the beam material, a is the crack length and h is the beam height measured from the crack tip. To simplify the test the beam is tapered (Fig. 1a) such that the terms in brackets in Equation 2 are a constant, m, so that

$$\mathcal{G}_{Ic} = \frac{4P_c^2m}{b^2E_b}. \qquad (3)$$

Note that the fracture energy is independent of crack length which is usually very difficult to measure.

To apply this technique to thick film adhesion, a *single* beam test specimen was devised. The beam shape, tapered for $m = 100$, is shown in Fig. 1b and was cut from brass plate ($E_b \sim E = 15.6 \times 10^6$ psi*). These beams were 1 in. (2.5 cm) long, 0.25 in. (0.63 cm) high at both ends and 0.08 in. (0.2 cm) thick and were dip-soldered on to 80 mil† wide thick film strips. The test pattern for screen printing is given in Fig. 2a. A schematic diagram of a beam soldered to a thick film strip is given in Fig. 1b. Note that there are "feet" at the beam ends which serve to position the beam over the

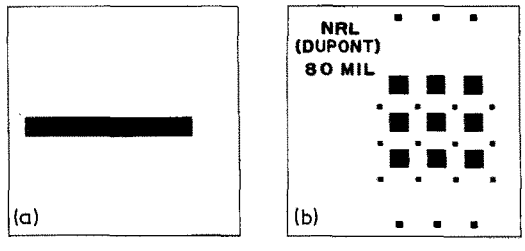

Figure 2 Screen patterns for (a) printing adhesive fracture test and (b) peel test metallizations.

* 10^3 psi $\equiv 6.89$ N mm^{-2}.
† 1 mil $= 10^{-3}$ in. (about 2.5×10^{-2} mm)

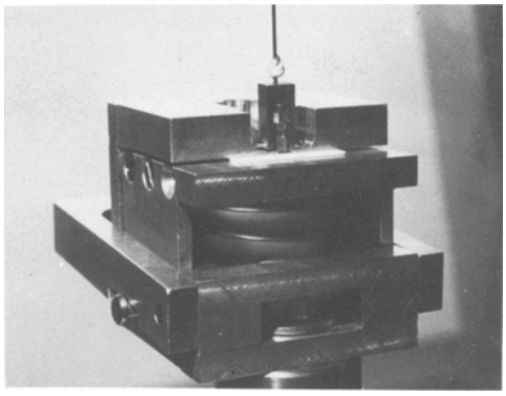

Figure 3 A single beam fracture test specimen mounted in the Instron test machine.

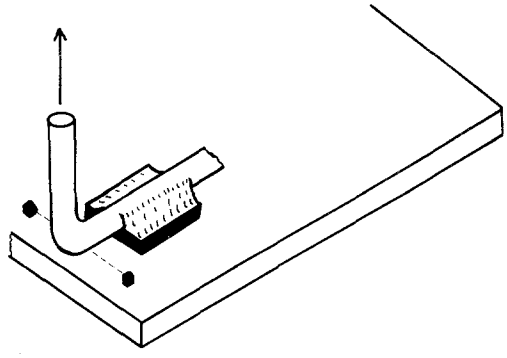

Figure 4 Schematic diagram of wire bond peel test.

film for soldering. The specimens were mounted in in the Instron test machine is shown in Fig . 3, by clamping the substrate in a holder on the lower cross arm and applying load to the beam via a hook through the loading hole.

It was found that consistent results could not be obtained using this technique unless a sharp pre-crack was introduced before testing. This is consistent with the established principle of fracture testing, that valid results cannot be obtained unless the initial notch or flaw has the tip radius ρ, characteristic of the material, i.e. a "natural" crack. This requirement can be met by initiating a crack and then arresting it immediately. A technique was devised to apply a lifting force at the beam end and a compressive force at the top of the beam simultaneously. This "bottle cap opening" action is illustrated in Fig. 1b. Usually, the formation of the pre-crack could be heard by a sharp snap, but, this noise was not always evident and failure to hear it might cause the operator to bend the beam excessively, a method was developed for observing crack formation by viewing the specimen in front of a strong light through a low-power microscope.

2.2. Solder-bond peel test

Measurements of thick film peel adhesion strength were made using the method specified by the Electronics Products Divison, I. E. duPont de Nemours and Co [7]. The test pattern is shown in Fig. 2b and consists of dip-soldering wires (No. 22, Sn-coated Cu magnetic) to the thick film pads.

Wires were soldered to the test plate by positioning along one of the rows of metallization pads. The free end of each wire was then bent perpendicular to the plate (Fig. 4) and pulled from the pads sequentially using an Instron tensile test machine. Ideally, nine data points could be obtained from each plate, but the actual number was less because occasionally a bond would break when positioning the sample on the test machine, or two or three of the bonds would break simultaneously.

2.3. The metallizations

The two conductor inks examined in this study are listed in Table I along with the firing temperatures. The optimum firing temperature specified by the manufacturer is indicated. The solders used to bond the fracture test beams were 63Sn/37Pb for the Pt–Au films and 70Sn/18Pb/12In for both the Pt–Au and the Au films. The numerical values in the solder composition refer to the wt% of each element and the tin–lead–indium solder was prepared by Semi-Alloys Co, Mt. Vernon, New York. In the peel tests only the Pt–Au metallization with 63Sn/37Pb solder was studied. The flux used in all solderings was LA-Co Nonacid (Lake Chemical Co, Chicago).

The ceramic substrates were 96% alumina (AISIMAG, American Lava Co., Tennessee) measuring 1 in. × 1 in. × 0.025 in. and were used as received without any cleaning. Printing of the

TABLE I Thick film adhesion test results

Firing temperature (°C)	Peel strength (g)	Fracture energy $\mathcal{G}_{Ic}$ (J m^{-2})
Pt–Au† –63 Sn/37 Pb		
755° C	840 ± 275	32 ± 29
* 860	840 ± 245	46 ± 37
950	670 ± 250	5.7 ± 3.4
Pt–Au† –70 Sn/18 Pb/12 In		
860	–	88 ± 40
Au‡ –70 Sn/18 Pb/12 In		
800	–	45 ± 37
* 900	–	63 ± 55

* recommended temperature
† duPont 7553
‡ duPont 8380

metallizations was done using a Presco Model 100c screen printer (200 mesh), (modified, Bound Brook, New Jersey), and the firing furnace was a 4-zone belt model built by BTU Engineering, Waltham, Mass. The total firing time was 1 h with ~ 10 min at the peak temperature.

2.4. Post-failure examination

The fracture surfaces of the films left on the substrate were examined using scanning electron microscopy (SEM, Advanced Metal Research, Model 1000) and the elemental composition was determined simultaneously using electron dispersive X-ray analysis (EDXA, Kervex Corp, Model 1500).

3. Results

3.1. Fracture energy and peel strength

The average test values are listed in Table I. It is quite evident that neither set of data provides an unambiguous indication of the optimum firing temperatures, especially in view of the large standard deviation of the results. In fact, this level of error is suspicously high even for fracture test results, which generally show large scatter. Consequently, the data were subjected to statistical analysis by plotting on Gaussian probability paper. In Fig. 5 and 6 the probability plots indicate a bimodal distribution for much of the test data. A very distinct separation of the data for the 860° C fired Pt–Au film soldered with Pb–Sn is shown in Fig. 5, and the peel data for this film–solder combination fired at 860° C also gave a clear separation in the probability plot in Fig. 6. The results separated into the average high and average low values are presented in Tables II and III. The statistical analysis has clearly reduced the standard deviation especially for the fracture energy values. It is also

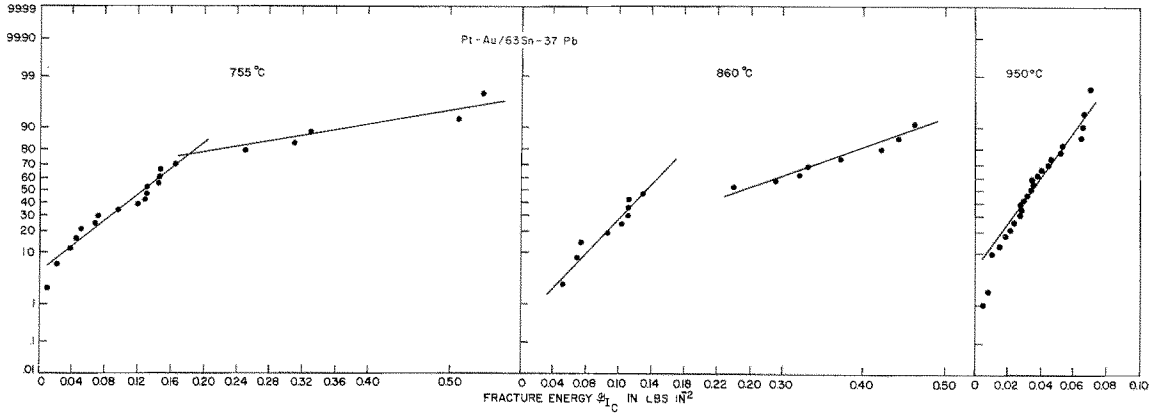

Figure 5 Probability plots of adhesive fracture data for the Pt–Au/Pb–Sn tests.

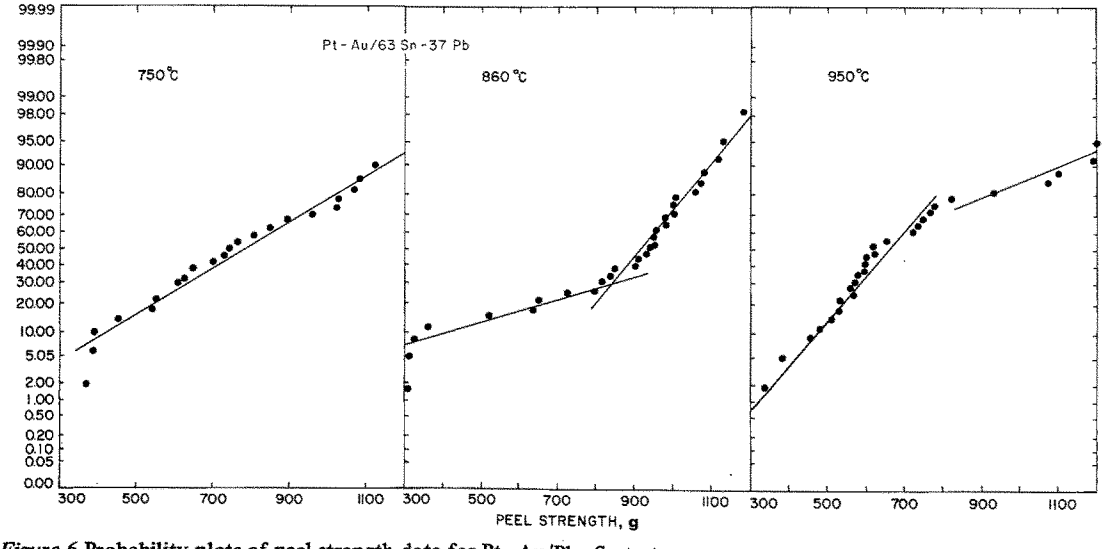

Figure 6 Probability plots of peel strength data for Pt–Au/Pb–Sn tests.

TABLE II Statistical analysis of fracture energy data $\mathcal{G}_{Ic}$ (J m^{-2})

Firing temperature (°C)	High values	Low values	Number of specimens
Pt–Au†–63 Sn/37 Pb			
755	74.0 ± 28.0 (25%)	17.5 ± 9.0 (75%)	24
860	60.5 ± 14.5 (50%)	17.0 ± 4.0 (50%)	18
950	–	5.80 ± 3.0 (100%)	25
Pt–Au†–70 Sn/18 Pb/12 In			
860	86.0 ± 30.0 (100%0	–	20
Au‡–70 Sn/18 Pb/12 In			
800	64.0 ± 33.0 (63%)	12.5 ± 6.0 (37%)	19
900	64.0 ± 42.0 (85%)	7.5 ± 3.0 (15%)	30

† duPont 7553 ‡ duPont 8380

TABLE III Statistical analysis of peel strength data for Pt–Au†–63 Sn/37 Pb

Firing temperature (°C)	Peel strength (g)		Number of specimens
	High values	Low values	
755	–	780 ± 250 (100%)	23
860	1000 ± 90 (63%)	570 ± 215 (37%)	30
950	1120 ± 120 (20%)	600 ± 120 (80%)	30

† duPont 7553

worth noting that for both the $\mathcal{G}_{Ic}$ results and the peel strengths at different firing temperatures and even between different film–solder combinations, the high values are comparable and the low averages are also about the same. Indeed, the differences in the overall averages in Table I before the statistical analysis appear to be the result of differences in the ratio of high to low peel strengths or fracture energies.

In a similar study [8] using a constant-moment test configuration (which also allows $\mathcal{G}_{Ic}$ to be measured independent of crack length) the fracture energies did not show a bimodal distribution but gave a single distribution of $\mathcal{G}_{Ic}$ values equivalent to the low distribution of this study. It is believed that the difference lies in the manner in which the fracture tests are conducted as is discussed below.

3.2. Post-failure examination

All of the peel and fracture test failures occurred very close to the thick film/substrate boundary. However, the loci of failure were clearly in the metallizations, not the alumina substrate, since a haze of film was always evident on the specimens. In addition, small round patches of what appeared to the unaided eye to be solder were randomly distributed over the metallization failure surfaces from the fracture tests. These solder patches were not observed on the peel test failures.

It was further observed in the pre-SEM examination that the Pt–Au/Pb–Sn fracture surfaces of the films fired at 755° C had a relatively dark coloration and that the coloration was progressively lighter for the 860 and 950° C fired samples. It appeared that failure occurred closer to the substrate with increasing firing temperature and this judgement was later confirmed in the microscopic examination.

A detailed SEM study was made of the failure surfaces of the fracture test specimens in an effort to find distinguishing differences between the different film compositions, firing temperatures and high and low $\mathcal{G}_{Ic}$ values distinguished by the statistical analysis. The fracture surfaces were quite complex but it was possible to identify specific features common to many of the specimens, which are believed to be pertinent to film morphology and fracture behaviour.

3.3. Features

(1) Solder patches: These features have been mentioned already and are illustrated in Fig. 7. The upper surface of the patches bear no evidence of fracture or yielding, which suggests there had been no contact with the brass beam presumably due to air entrapment during the soldering process. Evidently, as the fracture proceeds along the lower film/substrate boundary it is locally disturbed at

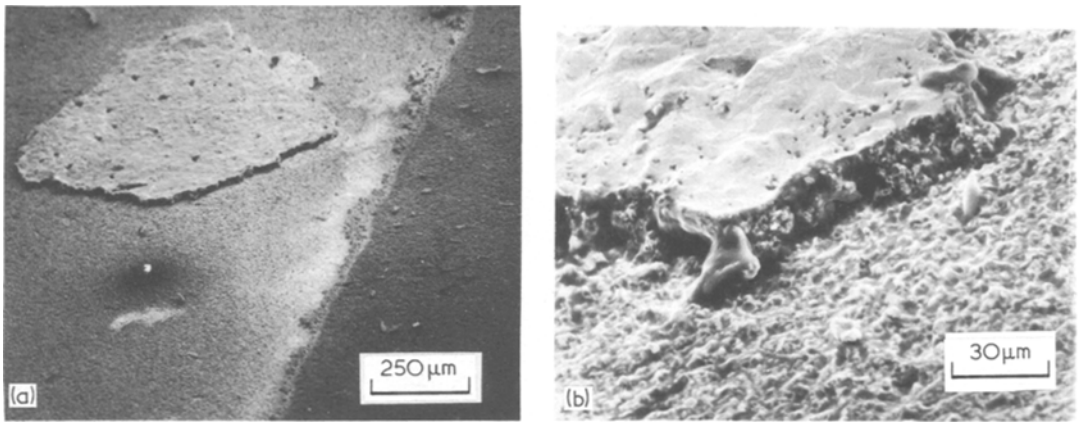

Figure 7 SEMs of solder patches. Note granular structure of thick film material under the solder layer.

these regions of disbond with the beam and tears vertically through the film and solder. The vertical wall of the solder patches reveal the usually granular structure of the metallization material (Fig. 7).

(2) Glassy and craterous fracture: The principal plane of failure was generally near the film/substrate boundaries and there were two features common to these areas of fracture. The first had the appearance of fractured glass or mineral, illustrated in Fig. 8a. Associated with these regions of glassy fracture was a craterous feature, such as shown in Fig. 8b which appeared to be sockets rimmed by thin ridges of glass. The glassy fracture regions and the craters were generally found together as interweaving networks but with one or the other more predominate depending on the film type and firing temperature.

(3) Conglomerate: On some specimens, granular material was observed on the principal failure planes. An example is shown in Fig. 9a which appears to be fragments of the conductive material (partially sintered metals and glass).

(4) Glaze: In one instance, the Au film soldered with Sn–Pt–In and fired at 900° C, the principal failure surface had relatively little of the glassy fracture or crater features, but instead had the appearance of a broken layer of glaze (Fig. 9b).

3.4. EDXA results

The SEM investigation of the fracture surfaces included an EDXA analysis of the various fractographic features. The elemental analyses are given in Table IV for the Pt/Au–Pb/Sn tests. As expected, the predominate constituents of a solder patch (taken through the top) were Pb and Sn although elements of the metallization such as Pt, Au, Bi and Si were also detected partly because the X-ray emission comes from depths of as much as 1 μm. On the other hand, the aluminium of the substrate was not detected through the solder. The conglomerate material contained all of the elements expected in the metallization including Zn and Cl, probably from the solder flux, and Pb and Sn whose presence indicates penetration of the solder into the film. Analysis of the glassy fracture regions indicated primarily the glass forming elements Bi

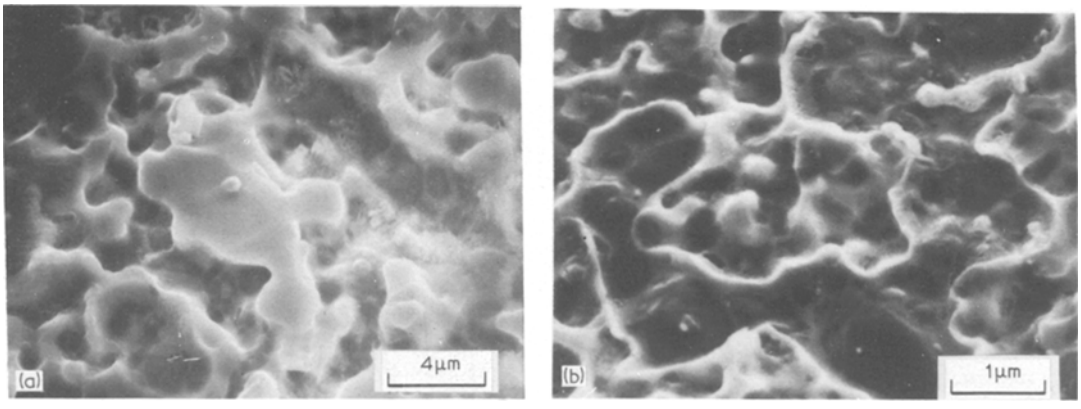

Figure 8 SEMs of (a) conchoidal fracture and (b) crater fracture features.

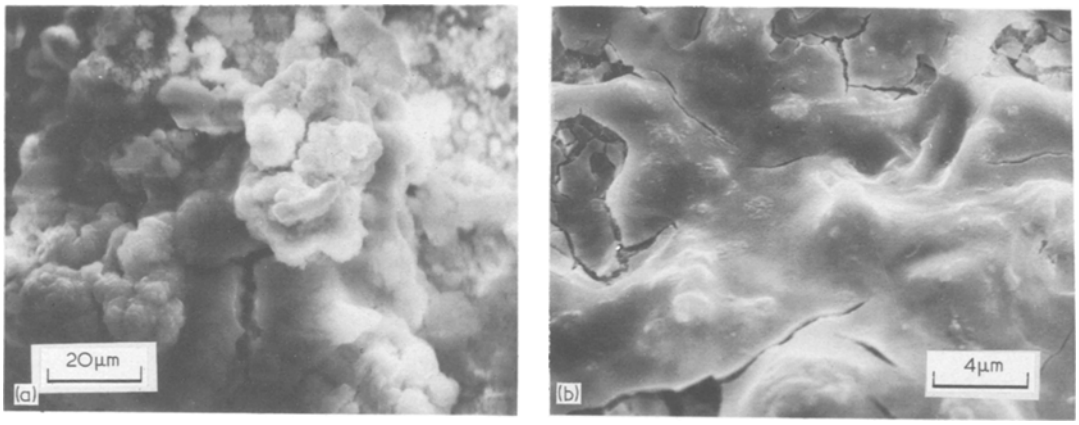

Figure 9 SEMs of (a) conglomerate and (b) glaze fracture.

and Si, and small concentrations of Pt and Au as well. The aluminium signal was strong for both the glassy and carter surfaces suggesting the close proximity of the underlying alumina and perhaps some solution of Al_2O_3 from the substrate into the glass. In fact, the EDXA spectra of the craters was nearly identical to that of the substrate except for trace amounts of the metallization elements.

3.5. Fractographic features of the test specimen

Pt–Au/Pb–Sn

755° C firing – Surfaces were completely covered by conglomerate material indicating failure in the film material. No evident distinction between high and low $\mathcal{G}_{Ic}$ tests.

860° C firing – Mixed glassy and crater fracture surfaces with glassy areas predominating. Possibly a greater amount of glassy surface on high $\mathcal{G}_{Ic}$ tests compared to low value specimens.

950° C firing – All specimens characterized by predominance of crater type fracture.

Pt–Au/Sn–Pb–In

860° C firing – Predominance of glassy fracture surface with some areas of failure in the overlaying conductive materials.

Au/Sn–Pb–In

800° C firing – Failure principally in conductive material with some areas of glassy and crater fracture surface. Conductive material on low $\mathcal{G}_{Ic}$ test surfaces was incompletely sintered in that rectangular particles containing mostly Au could be distinguished from spheres containing mostly Bi and Si.

900° C firing – Largely glassy fracture surface with some conductive failure. Low $\mathcal{G}_{Ic}$ test specimens were characterized by glaze surface (Figure 10b) although this feature was not entirely absent from the high $\mathcal{G}_{Ic}$ surfaces.

4. Discussion

Hitch [2, 3] has investigated the morphology of the fired films of Au conductor inks by mercury leaching of the metal from the glassy layer. He established that the glass wets the substrate to form a more or less continuous layer but with

TABLE IV EDXA analysis of fracture surface features

Element	keV	Substrate	Solder	Conglomerate	Conchoidal fracture	Crater
Al	1.52 ($K\alpha$)	very strong	–	moderate	strong	strong
Si	1.78 ($K\alpha$)	very weak	moderate	moderate	moderate	very weak
Au, Pt	2.14 ($M\alpha$)	–	moderate	moderate	weak	very weak
Pb, Bi	2.48 ($M\alpha$)	–	strong	strong	strong (Bi)	weak
Cl	2.64 ($K\alpha$)	–	–	strong	–	weak
Sn	3.48 ($L\alpha_1$), 3.72 ($L\beta_1$), 3.92 ($L\beta_2$)	–	strong	strong	–	very weak
Zn	8.66 ($K\alpha$)	–	–	moderate	–	very weak
Pt	9.50 ($L\alpha_1$)	–	weak	weak	weak	very weak
Au	9.72 ($L\alpha_1$)	–				
Pb	10.58 ($L\alpha_1$)	–	weak	weak	–	–
Bi	10.84 ($L\alpha_1$)	–	–	–	weak	weak
Au	11.50 ($L\beta_2$)	–	weak	–	–	–

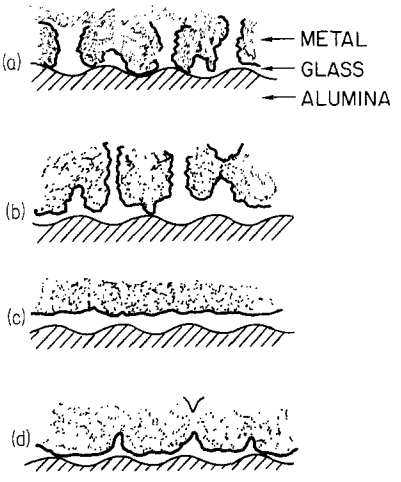

Figure 10 Schematic diagrams of (a) the metal/glass interface illustrating strong interlocking, (b) weak interlocking, (c) metal-glass phase separation, (d) gravitational flow-out of glass.

columns of glass extending into the metallic layer as illustrated in Fig. 10a. If the film is overfired either by too long at temperature or too high a temperature, the glass flows out of the metallic phase to reduce the degree of interlocking as in Fig. 10b. In extreme cases, complete separation of the glass may occur as in Fig. 10c. Since the noble metal constituents are more dense than the glass, the migration of the latter into the film/substrate boundary must be driven by surface forces. Hitch suggested that optimum film adhesion is obtained when there is a high degree of interpenetration of the two phases and a minimum development of a continuous glassy phase, so that failure could not proceed by brittle (low energy) fracture through glass without intercepting high fracture energy regions of metal.

The test data and fractography of the work here fully support and amplify the results of Hitch. The results with the Pt–Au/Pb–Sn system appear to cover the spectrum of behaviours expected of the morphologies of Fig. 10. At a firing temperature of 755° C, 105° below the recommended temperature, the majority of the specimens had low $\mathcal{G}_{Ic}$ values (and peel strengths) and failure was in the metallization. Evidently, underfiring had prevented the formation of any significant glassy bonding layer and separation took place between partially sintered components.

Firing of the Pt-Au metallization at the recommended temperature of 860° C produced a larger percentage of high $\mathcal{G}_{Ic}$ specimens and glassy fracture dominated their failure surfaces. This fractographic feature is believed to correspond to the highly interlocked configuration of Fig. 10a, with fracture occurring through the glass columns accompanied by pull-out of the metallic regions in that conductive granules were left on the surface or there were pockets in the glass layer from which granules had been removed. The Pt–Au film fired at 860° C but soldered with Pb–In solder exhibited a similar failure mode and accordingly gave high $\mathcal{G}_{Ic}$ values.

Overfiring of the Pt–Au film at 950° C led to a craterous glass layer which suggests flow-out of the glass and probably gravity driven flow up from the film/substrate boundary toward the film/air interface leading to the situation depicted in Fig. 10d. EDXA analysis of these surfaces support the view that the glass layer is quite thin, especially at the bottom of the craters (Table IV). Such flow requires incomplete consolidation of the conductive network above the glass layer.

The gold metallizations (soldered with Sn–Pb–In) were largely underfired at 800° C. The loci of failure were predominately in the metallization and the EDXA indicated poor consolidation of the constituents. At the recommended temperature, 900° C, glassy fracture with some failure in the conductive layer was observed, characteristic of an interlocked boundary between metal and glass. The low $\mathcal{G}_{Ic}$ values of the 900° C fired film exhibited glaze fracture which suggests overfiring and complete separation of glass and noble metal phases as illustrated by Fig. 10c. Evidently, there was better consolidation of the metallic constituents of the Au film thereby preventing upward flow of glass as occurred with the overfirng of the Pt–Au film.

Although it was possible to distringuish fractographic differences between films fired at different temperatue, clear fractographic distinction between the statistically determined high and low $\mathcal{G}_{Ic}$ values at a given firing temperature were not always evident. This failure to discern any physical reason for the bimodal distribution of fracture energies and peel strengths means we must examine some plausible, though speculative, explanations for the phenomena. The argument that it is an artifact of the fracture test can be dismissed out of hand, since the peel data also show a bimodal distribution and both show nearly the same quantitative distribution of data for the 860° C fired Pt–Au/Pb–Sn system.

It is important to understand that there is not necessarily a one-to-one correspondance between the fracture energy, $\mathcal{G}_{Ic}$, and the overall fractogra-

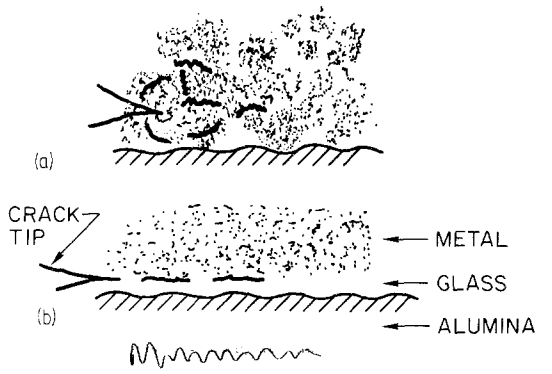

Figure 11 Crack tip damage zones.

phic appearance of the failed surface. The value of $\mathcal{G}_{Ic}$ is governed by the events (micro-cracking) that occur in the immediate vicinity of the tip of the pre-crack as load is applied to the specimen. The nature and extent of this damage zone is determined by the film morphology and composition near the pre-crack front. Once a certain level of damage has developed, dependent on film properties, the entire crack front advances spontaneously and the specimen fractures. Two situations of crack initiation (i.e. development of the damage zone) are illustrated in Fig. 11; (a) a pre-crack in the film/substrate boundary where there is extensive interlocking of the metal and glass phases and extensive micro-cracking through the metal phase must precede spontaneous advance of the main crack front, (b) micro-cracking essentially coplaner with the pre-crack. The two cases are distinguished by the size of the crack tip damage zone. It was not possible to locate the pre-crack region on any of the fracture surfaces examined so that the film structure in which the propagation initiated could not be identified. Presumably, the level of crack tip damage associated with slow crack growth and the subsequent damage occurring during spontaneous propagation were essentially the same.

It is important to recognize that the film morphology varies over the film area. Consequently, the fracture energy will depend on the film structure from which the crack happens to initiate. Therefore, for a sufficiently large sampling, the $\mathcal{G}_{Ic}$ results should reflect the statistical variation in film morphology. From the bimodal distribution of the data it follows that at the recommended (optimum) firing temperature a greater proportion of the film area of each specimen develops the morphology for optimum adhesion, i.e. a highly interlocked boundary between glass and metal, but that a significant proportion of the film area is under or overfired and thus poorly adherent. At firing temperatures other than optimum the converse is true; the greater proportion of the film area adheres poorly, some area of good adhesion may exist. It is not a matter of some specimens being good and others bad: if that were the case there would have been a clearer fractographic distinction between the "high" and "low" fracture energy specimens.

As was mentioned earlier, fracture tests of these same thick film metallizations using an applied moment test specimen [8] did not show a bimodal distribution but gave $\mathcal{G}_{Ic}$ values corresponding to the low distribution observed here. The constant compliance and applied moment tests differ in one important aspect; the stress distribution at a crack tip in an applied moment specimen which is a double beam test is more symmetrical than in the *single beam* constant compliance specimen, since for the latter only one arm experiences bending displacement (as in the peel test). This asymmetry of the strain field may tend to direct cracking away from the interface up into the film (high $\mathcal{G}$ region) so that propagation is more likely to occur in metal-reinforced glass for the constant complance and peel tests than for the applied moment test. Consequently, the constant compliance test may be more sensitive to differences in film morphology.

Whatever the explanation for the bimodal distribution, its existence is a serious matter as far as the reliability of thick-film microelectronic devices is concerned. It suggests for example that 40 to 50% of a metallization fired at the recommended temperature can have anomalously low adhesion strengths. In other words, nearly half the solder-bonded connections along a metallization strip would be half as strong as the other connections. It should be emphasized that this problem is not necessarily characteristic of thick film technology as a whole, but may be peculiar to the specimens prepared at this laboratory.

It is instructive to consider the observed fracture energies quantitatively, and relate them to the peel strength results. The fracture energies of glasses and ceramics are on the order of 5 to 15 $J\,m^{-2}$ [11], and for those films where failure was judged to have occurred in a glassy layer (Pt–Au/950° C and the low $\mathcal{G}_{Ic}$ values for Au fired at 900° C) the $\mathcal{G}_{Ic}$ results are within this range. The high $\mathcal{G}_{Ic}$ values were in the 60 to 90 $J\,m^{-2}$ range which is well above that characteristic of inorganic glasses but very much lower than the fracture energy of

metals ($> 1000\,J\,m^{-2}$). Moreover, fracture of these metals would involve ductile deformation for which there was no SEM evidence. A more likely explanation is that the metal phase of the films prevent crack development along a single plane, so that micro-cracking and the development of a damage zone (Fig. 11a) must occur before crack propogation. The actual energy per unit area may be the same as for glass fracture, but the load on the specimen must be continuously increased until the damage zone reaches some critical size, giving a large apparent fracture energy, even though the failure may still be in the glass.

Inspection of Equation 2 indicates that if the failure mode of the fracture test and the peel test are the same then peel strength $\propto \sqrt{\mathcal{G}_{Ic}}$.
This relationship appears to be correct since the ratio of high and low peel strengths are generally equal to the square root of the ratio of the corresponding high and low $\mathcal{G}_{Ic}$. For example, the peel strength ratio for the Pt–Au/Pb–Sn system fired at 860° C is 1.8 and the square root ratio of $\mathcal{G}_{Ic}$ is 1.9. The relationship can be carried further by considering the peel test, itself, as a single beam fracture test and using Equation 2 to compute an effective crack length. Taking the beam width b, and beam height h, as equal to the wire diameter and the peel strength as P_c, the high and low $\mathcal{G}_{Ic}$ values for the Pt–Au/Pb–Sn–860° C system give 0.052 in. (0.132 cm) and 0.056 in. (0.143 cm) respectively for the crack length a. This distance corresponds to the unbonded length of the peel test wire from the center line of the vertical wire to the edge of the metallization pad, nominally 0.050 in. [7]. Thus, the peel test is a fracture test with the unbonded arm length as the effective crack length.

This calculation indicates the possible predictive value of thick film $\mathcal{G}_{Ic}$ data for estimating solder (and other) bond strengths. If the geometry of the attachment approximates a beam or other such configuration for which there is an expression such as Equation 2 relating P_c and $\mathcal{G}_{Ic}$, then the bond strength can be calculated. If such estimates prove to be generally reliable, then fracture mechanics could be a useful tool in the design of microelectronic devices.

5. Conclusion

This study has demonstrated that a fracture mechanics approach can be successfully used to characterize the adhesion of thick film metallization. In comparison with the peel test, the fracture test is insufficiently more discriminating to warrant its use for quality control purposes, especially in view of the greater experimental complexity of the fracture test. In research work, the fracture approach has the advantage of providing fracture energies for comparison with those of the film constituents, and fracture results have at least the potential of being used for design purposes.

In addition to demonstrating the feasibility of thick film fracture testing, this study has added support to the morphological description of thick films developed by Hitch. The question of bimodal strength distribution revealed by both the peel and fracture tests needs to be pursued.

Acknowledgements

The authors wish to express their appreciaiton to Dr J. S. Murday and Dr P. F. Becher of the Naval Research Laboratory for many useful discussions during the course of this work. Appreciation is also extended to Mr. L Mann of the Space Sciences Division NRL, for preparation of the thick film samples, and Mr J. W. Willis of the Naval Air Systems Command, which funded this work.

References

1. R. W. VEST, "Conduction Mechanisms in Thick Film Microcircuits", Semi-Annual Technical Reports, (Purdue University, Indiana, 1971–1975).
2. T. T. HITCH, Proceedings of the International Society for Hybrid Microelectronics Symposium, (1971) p. 7.7.1.
3. *Idem, J. Elect. Mater.* **3**, 553 (1974).
4. W. D. BASCOM, C. O. TIMMONS and R. L. JONES, *J. Mater. Sci.* **10**, (1975) 1037.
5. D. W. HAMER and J. V. BIGGERS, "Thick Film Hybrid Microcircuit Technology" (Wiley, New York, 1972) p. 132.
6. D. S. CAMPBELL, in *"Handbook of Thin Film Technology"*, Edited by L. T. Maissel and R. Glang (McGraw-Hill, New York, 1970).
7. Method of Testing for Wire Peel Adhesion of Soldered Thick Film Conductors to Ceramic Substrates, E. I. duPont d Nemours & Co, Inc, Wilmington, Delaware, Bulletin A-74672, 3/71.
8. P. F. BECHER and W. L. NEWELL, *J. Mater. Sci.*
9. S. MOSTOVOY and E. J. RIPLING, *J. Appl. Polymer Sci.* **10**, (1966) 1351.
10. W. D. BASCOM, R. L. COTTINGTON, R. L. JONES and P. PEYSER, *ibid* **19**, (1975) 2545.
11. R. L. COBLE and N. M. PARIKH, in "Fracture, An Advanced Treatise", Vol. 7 edited by H. Liebowitz (Academic Press, New York, 1972) p. 243.

Received 17 September and accepted 22 November 1976.